

Tissue engineering of blood vessels using three-dimensional bioprinting of endothelial and smooth muscle progenitor cells
PN-III-P1-1.1-PD-2016-1660, No. 19/2018 acronym BIOPRINT,
Phase report III-2020

Introduction

3D Bioprinting is a technique used for manufacturing tissues and organs that mimic the architecture of natural tissues. 3D bioprinting combines cells, growth factors and biomaterials to create a setting in which cells grow and differentiate into native tissue-like structures. In 3D bioprinting, biomaterials are printed layer by layer to produce structures similar to a desired organ or tissue. The first patent for this technology was proposed in the United States in 2003 and granted in 2006 [1]. Bioprinting involves several steps: (i) biomaterial selection, (ii) designing the bioprinting model/scaffold using CAM software, (iii) bioprinting the model using proper bioprinting technique, and (iv) analyzing bioprinting constructs [2]. In 3D bioprinting an exhaustive knowledge and methodology approach is needed from various fields such as engineering, stem cell biology, tissue engineering, and biomaterials science to create an ideal model [3]. An ideal scaffold should be biocompatible, non-immunogenic, non-toxic, anti-thrombotic, with vasoactive properties, allowing the remodeling of the scaffold post-implant by the host tissue. To create such a scaffold, physicochemical parameters such as geometry, pore size, surface properties, adhesion, degradation and biocompatibility should be analyzed [2-4]. Although there is a wide variety of biological materials, including synthetic polymers, hydrogels, extracellular matrix, cell aggregates, and microcarrier structures, several aspects have to be considered for obtaining structures similar to the target tissue. First of all, an important aspect is *compatibility* of biomaterials with different types of printing technologies. Extrusion printing is the most flexible method due to the simple mechanism and the larger diameters of printheads. Drop or laser printing is only used for hydrogels. The second aspect is the *bioprintability* of scaffolds. In this case, the bioprinting of hydrogels is superior to other bioinks. The third aspect is *replicability*, which implies that the constructs should be as close as possible to the desired tissue. Cell interactions and proliferation, scaffold degradation, are also important for tissue formation. The fourth aspect is related to the *bioprinting resolution*, which depends on bioprinting type as well as on bioink.

Laser bioprinting of hydrogels has a resolution of 5-10 μm , while the drop or extrusion bioprinting between 50-100 μm . The fifth aspect is *accessibility*. Matrigel™, collagen and fibrin hydrogels are more expensive compared to synthetic polymers. In a scaffold, hundreds of millions of cells are needed so that obtaining them could be intensive, costly and time-consuming. Other aspects involve: *scalability, practicality, mechanical and structural integrity, degradability, commercial availability, immunogenicity and applicability*.

Despite the multitude of biomaterials that appear regular, relatively little research has been devoted to the development of biomaterials for the bioprinting process. Although a large number of hydrogels have great potential for tissue engineering, only a limited number can be used in bioprinting due to the lack of bioprintability and toxicity of degradation products. Also, the bioprinter parameters that should be optimized for each specific tissue. The main objectives for improving bioprinting are to minimize cell loss, promote cell-cell interactions, increase mechanical properties, and biocompatibility of 3D bioprinting scaffolds. Amniotic fluid cells are a heterogeneous population of mesenchymal cells of fetal origin of great importance in regenerative medicine. This population is known to have low immunogenicity, so it is less likely to generate an immune response thus having a high therapeutic potential [5, 6]. Phenotypes found in cell culture in amniotic fluid include epithelial-like and fibroblast-like cells [7]. There are also approximately 0.1-0.5% stem cells defined by c-kit expression (CD117+) on the cell surface. The regenerative potential of amniotic fluid-derived mesenchymal stem cells (AFSC) arises from their ability to differentiate and reduce immunogenicity [8]. AFSC can differentiate into different cell lines, such as endothelial [9], cardiac [10], neural, bone [11]. AFSC can also be reprogrammed without the use of gene transfer technology for induction of pluripotent stem cells [11]. The literature suggests a strong correlation between AFSC and the cardiovascular system. AFSC have demonstrated the ability to form capillary-like networks when grown in hydrogels and there is also evidence of paracrine signaling when AFSC are indirectly co-cultivated with human cardiac cells thereby modulating cardiac regeneration [12, 13].

Cardiovascular diseases are the leading causes of mortality worldwide and require over one million bypass / blood vessel replacements annually in the United States alone [14]. Although autologous vascular grafts are the gold standard for clinical use, they are not suitable for a large number of patients due to vascular disease, amputations or previous vascular tissue harvesting.

Despite the clear clinical needs of vascular substitutes, currently available synthetic grafts (for example, Dacron and Teflon) have proven to be successful only in large caliber implants; small diameter vascular substitutes (<6 mm) have generally unsatisfactory results, with major negative side effects, such as acute thrombosis, hyperplasia and aneurysm [15]. Arterial failures are generally attributed to the relatively low blood flow rate in these small vessels, which increases the rate of interactions between cells and molecules in the blood and polymeric implants. Therefore, there are strict requirements regarding the biofunctionality of the small diameter designed grafts. In order to produce grafts with normal vascular functions, at least 2 requirements must be met: (1) a confluent endothelium providing a nonthrombogenic interface and (2) a smooth contractile muscle tissue that can withstand haemodynamic stress and local changes in blood pressure that occur through constriction and physiological relaxation of the vessel [16]. Tissue engineering has emerged as a promising alternative approach for viable small diameter arterial grafts. Various strategies including decellularized tissue, synthetic polymeric matrices, self-assembling cell layers and hydrogels have been used to create living vascular structures and replace native blood vessels; these strategies have achieved different levels of success. These approaches generally produce vascular substitutes in the form of a robust tubular matrix containing smooth vascular or fibroblast muscle cells followed by seeding and cultivation of endothelial cells to achieve reendothelialization. This multi-step construction process is slow and requires complicated procedures and long manufacturing periods. In addition, grafting and retention rate of endothelial cells is strongly influenced by seeding mode, surface properties, cell density and culture conditions and, therefore, current methods can hardly be considered reliable for generating an intact functional endothelium. Therefore, biomimetic reconstruction of blood vessels through tissue engineering remains a difficult task that requires new construction techniques [17-20]. An important advantage of 3D bioprinting is the ability to build tissue / organ equivalents with a structure as close as possible to the native one. The precise positioning of cell-loaded bioinks simulates the anatomical features of the target tissue / organ, so that as cells proliferate, migrate and differentiate into a biomimetic construct. In particular, coaxial extrusion technique can use various biomaterials for bioprinting resulting in vessel-like structures [21].

For the successful bioprinting of a functional vessel, an essential factor is the bioink used. It must be biocompatible with the different cell types and promote the functionality of the cells and also allow the direct bioprinting of the vessels. While the hydrogels used to create vessels (fibrin, elastin, collagen, fibroin) generally have poor printability, materials suitable for co-extrusion bioprinting (alginate, gelatin methacryloyl, photopolymerized hyaluronic acid) usually have negative results due to low cellular affinity or poor mechanical properties and the functionality of the tissues is impaired. Despite significant improvements of current technologies to create three-dimensional (3D) blood vessels, the formation of a functional engineered vascular system with multiscale vessel networks from capillaries to large vessels has remained challenging in this field. Inability in fabrication of 3D vascular networks has limited tissue engineering in the growth of thick tissue or organ-level constructs [22].

The aim of this project was to create vascular structures using collagen and hyaluronic acid hydrogels and endothelial and muscle progenitor cells derived from mesenchymal stem cells isolated from amniotic fluid using 3D bioprinting.

1. Amniotic fluid stem cells differentiation and characterization

The amniotic fluid cell cultures (AFSC) were kindly provided by Genetic Lab S.R.L. diagnostics laboratory upon informed consent of the patients in agreement with national and EU rules. The primary cultures were obtained by centrifugation of amniotic fluid at 1050 rpm for 10 min. The cells were then cultured for 10 days without passages at Genetic Lab in AmnioMax medium, with medium change every 2 days (ThermoFischer Scientific, Waltham, Massachusetts, USA), then delivered to IBPC ‘‘N. Simionescu’’.

1.1. Cell culture and differentiation conditions

After 10 days primary culture was passage and cultured in differentiation specific media supplemented with growth factors. Endothelial differentiation of AFSC was done by cultured in M200 Medium supplemented with 10% FBS (fetal bovine serum), 40 ng/mL vascular endothelial growth factor (VEGF), 20 ng/ml insulin growth factor (IGF-1), 10 ng/ml epidermal growth factor (EGF), 10 ng/ml basic fibroblast growth factor (bFGF), 100 µg /mL penicillin, 100 µg/mL streptomycin, and 50 µg/mL neomycin (all purchase from Thermo Fischer Scientific, Waltham, Massachusetts, USA).

Smooth muscle differentiation of AFSC was done by cultured in M231 Medium supplemented with basic FGF (2 ng/ml), EGF (0.5 ng/ml), heparin (5 ng/ml), IGF (2 µg/ml) and bovine serum albumin BSA (0.2 µg/ml) (Thermo Fischer Scientific, Waltham, Massachusetts, USA). The cells were maintained in these media for 4 weeks, and passage when reached subconfluence. Cell cultures were maintained at 37 °C with 5% CO₂ and 21% O₂ in a humidified atmosphere.

1.2. Flow cytometry assay

Flow cytometry was used for the assessing the expression of cell specific surface markers (Gallios, Beckman-Coulter, California, SUA). AFSC (1x10⁵ cells/marker) were stained with fluorochrome-conjugated (FITC - Fluorescein-isothiocyanate and PE - Phycoerythrin) primary antibodies against CD29 (integrin β1), CD31 (PECAM-1), CD49e (integrin α5), CD54 (ICAM-1), CD56 (NCAM), CD73, CD90 (Thy-1), CD105 (endoglin), CD146 (MCAM), and VEGFR2 (Beckman-Coulter). AFSC were detached using acutase (Sigma-Aldrich, St. Louis, MO, USA) and washed in phosphate-buffered saline solution (PBS). Cells were then incubated with the primary antibodies at room temperature in the dark for 30 min. Further, the cells were washed and centrifuged at 400g, 10 min, in PBS (Phosphate Buffer Solution) with 1 % BSA. For negative controls, AFSC were stained with the corresponding isotype-matched IgG antibodies (Beckman-Coulter, California, SUA). Flow cytometry data were analyzed using the Gallios software 1.0 (Beckman-Coulter, California, SUA).

1.3 Gene expression and functional characterization of endothelial progenitor cells (EPC)

Gene expression levels in AFSC and EPC were assessed by qRT-PCR. Total cellular RNA was isolated from cultured cells using RNeasy Mini Kit (Qiagen, Hilden, Germany) and reverse-transcription reaction was performed using M-MLV polymerase, High-Capacity cDNA Reverse Transcription kit (Thermo Fischer Scientific, USA). mRNA levels of endothelial associated genes (PECAM-1, ICAM-1, VE-Cadherin, eNOS and vWF) were quantified using TaqMan hydrolysis probes (ThermoFischer Scientific, Waltham, Massachusetts, USA). Quantitative Real Time-PCR reactions were carried out in a real-time thermocycler (ViiA7, Applied Biosystems, USA), following manufacturer's guidelines. The results were expressed using relative quantitation ($2^{-\Delta C_t}$), where ΔC^T represents C_T difference between values for AFSC and EPC.

Dil-Ac-LDL uptake assay. AFSC derived EPC were incubated with 6 µg/mL Dil-AcLDL-PE (Acetylated low-density Lipoprotein conjugated PE, ThermoFischer Scientific, USA).

Cells were incubated for 2 hours at 37 °C with 5% CO₂ and 21% O₂, washed with PBS and fixed with 1%PFA (paraformaldehyde) for 10 minutes at room temperature. **Ulex europaeus lectin (UEA) binding capacity to EPC.** For the assessment of Ulex europaeus agglutinin (UEA) binding capacity to EPC, cells were incubated with 0.01 mg/mL FITC – Ulex europaeus lectin (Sigma-Aldrich, St. Louis, MO, USA) for 2 hours, followed by a wash with PBS. The nuclei were counterstained with DAPI (1 mg/mL). The photomicrographs were taken with a digital camera Digital Net Camera DN100 using an Eclipse TE300 microscope (Nikon, Tokyo, Japan). **Matrigel vascular tubes assay.** To evaluate the formation of blood vessel networks in Matrigel, cells were seeded into 96-well plates at a density of 3,000 cells per well. Briefly, 50 µL of Matrigel (Sigma-Aldrich, St. Louis, MO, USA) was added in each well of a 96 well plates, and left to solidify for 30 minutes at 37°C. After Matrigel polymerization, cell suspension was added and incubated for 4 hours. Tubes formation was observed using an Eclipse TE300 microscope (Nikon, Tokyo, Japan) equipped with a digital camera (Digital Net Camera DN100).

1.4 Gene expression and electrophysiological analysis of smooth muscle progenitor cells (SPC)

mRNA levels of muscular associated genes (smoothelin, calponin 1, α -SMA (α -actin), Myh11 (myosin heavy chain), α -tropomyosin, caldesmon-1, Cav3.1) were quantified using TaqMan hydrolysis probes (ThermoFischer Scientific, Waltham, Massachusetts, USA).

In patch-clamp experiments we used borosilicate glass capillaries (GC150F-10, Harvard Apparatus, USA) pulled with a PUL-100 equipment (WPI, Sarasota, FL, USA) and fire-polished with a home-made microforge to yield a resistance in solution between 2-3 M Ω . The patch-clamp setup included an inverted microscope placed on an antivibratory platform in a Faraday cage, a stage temperature controller (TC202A, Harvard Apparatus, MA, USA), a resistive feedback amplifier (WPC-100, ESF electronic, Göttingen, Germany) connected to a Digidata 1322A AD/DA interface controlled by the pClamp8.2 software (Axon Instruments, Molecular Devices, Sunnyvale, CA, USA). Briefly, the extracellular solution was composed of: 135mM NaCl, 5.4 mM KCl, 1.8 mM CaCl₂, 0.9 mM MgCl₂, 0.33 mM NaH₂PO₄, 10 mM HEPES, 10 mM D-glucose pH 7.40 at 25°C titrated with NaOH. The pipette solution contained: 140 mM KCl, 5 mM EGTA, 10 mM HEPES, pH 7.21 at 25°C titrated with KOH. Multiple voltage protocols were applied, including: a general protocol for K⁺ currents with depolarization steps from -60 to +60 mV with a duration of 300 ms from a holding potential of -80 mV; a double voltage ramp protocol (from -

120 mV to +80 mV in 2 s and back to -120 mV at the same time, from a holding potential of -70 mV) (INS double-ramp); a protocol for voltage-dependent Na⁺ currents with depolarization steps from -60 to +40 mV with a duration of 6 ms from a holding potential of -100 mV; standard protocol 2 of voltage-clamp for the separation of the current of Ca²⁺ + type L from the current of Na⁺ voltage-dependent. We applied the following pharmacological compounds: iberiotoxin 100nM (Alomone Labs, Jerusalem, IL), phrixotoxin-1 280μM, DIDS (stilbene disulfonate) 100 μM, mibefradil 10 μM, and nifedipine 1 μM (Sigma-Aldrich, St. Louis, MO, USA).

2. Design, bioprinting and characterization of blood vessel constructs using collagen-hyaluronic acid hydrogels and EPCs and SPCs

A computer-aided design (CAD) software (BioCad, RegenHU, Switzerland) was utilized to create the 3D models for bioprinting. A G-code series of instructions to be used by the 3D bioprinter (3D Discovery, RegenHU, Switzerland). The 2 printheads (one with bioink and EPC and the second with bioink and SPC, respectively) moved according to G-code instructions depositing bioink on circular slides. Bioprinting parameters were: 0.2 mm diameter needle, 1.2 bar extrusion pressure, 1 mm/sec printhead speed rate, 18°C temperature. The diameter of vascular tubes was 2.5 mm, and thickness and height of each layer were 0.3 mm. A 5 seconds polymerization followed each bioprinted layer. The number of cells was 10 million cells/1 ml Coll-HA hydrogel. The amount was sufficient for printing 10 constructs.

2.1 Hydrogel preparation

Collagen hydrogel (H0) containing 2% peptides (collagen) used was purchased from RehenHu (Villaz-St-Pierre, Switzerland). Using this hydrogel, we developed other 2 hydrogels (H25, H50) by adding hyaluronic acid (MW 1-1.6 MDa, 1%, Sigma-Aldrich, St. Louis, MO, USA) in 2 different proportion, 25% and 50%, respectively.

2.2. Fourier-transform infrared spectroscopy (FTIR), Thermal gravimetric analysis (TGA) and Scanning Electron Microscopy (SEM)

FTIR spectra were recorded with a Nicolet iS50R spectrometer, at room temperature, in the measurement range 4000–400 cm⁻¹. Spectral collection was carried out in ATR mode at 4 cm⁻¹ resolution. For each spectrum, 32 scans were co-added and converted to absorbance using OmnicPicta software (Thermo Scientific).

The thermogravimetric measurements were made on a TGA 851e from Mettler–Toledo. The microbalance has a precision of ± 0.1 mg and was kept at constant temperature (22 °C) during analyses to avoid the variation of mass measurement with temperature. Samples with a mass between 1 and 3 mg were placed into 70 μ L alumina pans. Samples were heated between 25 and 800 °C at 10 °C/min under air flow (50 mL/min).

SEM imaging was obtained using the following protocol. The constructs were washed with PBS and fixed in 2.5 % glutaraldehyde for 1 hour at room temperature. Glutaraldehyde was then removed, and successive dehydration was carried out in ethanol (40 %, 60 %, 70 %, 80 %, 90 %, and 100 %) for 10 minutes each. SEM analysis was performed on a HITACHI S2600N electron microscope, at 25 keV, on samples covered with a thin silver layer.

2.3 Water uptake

Water uptake was performed to demonstrate the hydrogel swelling behavior in the presence of PBS (phosphate buffer saline). Bioprinted constructs were weighted after printing, then immersed into PBS and weighed at 10 min, 30 min, 1hr, 2hrs, 4hrs, and 8hrs, respectively. The absorption rate was calculated according to the formula:

$$\text{Water uptake} = \frac{W_w - W_d}{W_d (\text{g/g})} \times 100$$

where: W_w = construct weight after immersion in the fluid at time t ; W_d = construct weight before immersion

2.4 Enzymatic degradation

Enzymatic degradation of the constructs was assessed using collagenase type I and hyaluronidase. Bioprinted vascular constructs were introduced into culture medium (control constructs) and in collagenase type I and hyaluronidase medium (10 μ g/ml collagenase and 10 μ g/ml hyaluronidase, Merck, New Jersey, USA) and then weighed at different intervals time (10 min, 30 min, 1hr, 2hrs, 4hrs, and 8 hrs). Weight loss was calculated using formula:

$$\% \text{ Weight loss} = \frac{W_i - W_t}{W_i (\text{g/g})} \times 100$$

where: W_i = construct weight in collagenase free medium; W_t = construct weight in collagenase type I medium

3. Characterization of blood vessel constructs populated with EPCs and SMPs

3.1 Viability, morphology and oxidative stress assays

EPCs and SMPs behavior at 7 and 21 days after bioprinting was evaluated using LDH, GSH, and MTT assays, as well as SEM. Cellular viability after 7 days and 21 days was evaluated using an **LDH assay** (Pierce™ LDH Cytotoxicity Assay Kit, Thermo Fischer Scientific, Massachusetts, USA). Lactate dehydrogenase (LDH) is a cytosolic enzyme present in many different cell types. Plasma membrane damage is followed by the release of LDH into the cell culture media. LDH can be quantified by a coupled enzymatic reaction in which LDH catalyzes the conversion of lactate to pyruvate via NAD⁺ reduction to NADH. Diaphorase then uses NADH to reduce a tetrazolium salt to a red formazan product that can be measured at 490 nm. Briefly, 50µL of each sample medium was transferred to a 96 well plate and then add 50µL of Reaction Mixture. The plate was incubated at room temperature for 30 minutes protected from light. Then was added 50µL of Stop Solution to each sample well and mixed by gentle tapping. The absorbance was measured at 490nm and 680nm using TECAN Infinite M200 (Männedorf, Switzerland).

Cellular stress was evaluated using **GSH assay** (Glutathione Fluorescent Detection Kit, Thermo Fischer Scientific, Massachusetts, USA). Glutathione (GSH) is an antioxidant found in eukaryotic cells. Reactive chemical species can cause a drop in GSH levels either by oxidation or reaction with the thiol group. A change in GSH levels is important for assessing toxicological responses and can promote oxidative stress, potentially leading to apoptosis and cell death. The protocol followed the manufacturer specification, using a standard for absolute quantification. The fluorescent emission was read at 510 nm, with excitation at 390 nm using a TECAN Infinite M200 spectrophotometer (Männedorf, Switzerland).

The viability and proliferation were assessed using **MTT assay** (Vybrant® MTT Cell Proliferation Assay Kit, Thermo Fischer Scientific, Massachusetts, USA). The assay is a colorimetric method that allows quantitative assessment of proliferation, cell viability and cytotoxicity. The viable cells reduce yellow tetrazolium salt MTT (3-(4,5-dimethylthiazol-2-yl)-2,5-diphenyltetrazolium bromide) to a dark blue formazan via mitochondrial enzymes. Briefly, the constructs cultivated for 7 days and 21 days respectively in 24-well plates, were incubated with 15 µl Solution I (MTT) at 37°C for 4 hours. Solution II (containing solubilization agents SDS and HCl) was added and pipetted vigorously to solubilize formazan crystals. After 1 hour the absorbance was read at 570 nm (TECAN Infinite M200, Männedorf, Switzerland).

The cellular morphology and distribution were evaluated using SEM, following the protocol described under 2.2 materials and methods section.

3.2 ELISA and Griess assay

The secretion of VEGF A from the endothelial progenitor cells at 7 days and 21 days of culture in the constructs was measured using Human VEGF ELISA kit (Sigma-Aldrich, St. Louis, MO, USA) according to manufactured protocol. Nitric oxide (NO) was measured spectrophotometrically at 548 nm using the Griess Reagent Kit for Nitrite Determination (Molecular Probe, Thermo Fischer Scientific, Massachusetts, USA).

3.3 Immunohistochemistry

Immunohistochemistry was performed on 5 μm -thick cryosections on constructs at 21 days post-bioprinting. The sections were then incubated overnight, at 4°C, with the following primary antibodies: monoclonal mouse anti-human CD31 (1:250), CD144 (5 $\mu\text{g}/\text{mL}$), smoothelin (1:100), and anti-human $\mu\text{tropomyosin 1}$ (1:100) (Invitrogen, Thermo Fischer Scientific, Massachusetts, USA). The slides were washed three times with PBS, for 10 min., and then incubated for 2 hours at room temperature, with the secondary antibodies. The pictures were taken using an inverted microscope with an incorporated digital camera system for imaging (Olympus CKX41 equipped with Sense XC30 camera, Shinjuku, Tokyo, Japan).

Data analysis

Data are expressed as mean \pm standard deviation (SD) or mean \pm standard error of the means (SEM), as appropriate. In all instances "n" signifies the number of cells analyzed in a certain experimental condition. Statistical analysis was performed using Student's t test or Fisher's exact probability test, using a critical level of $p < 0.05$. For immunophenotyping and gene expression profiling, statistical analysis was performed using the one-way ANOVA method for correlated samples.

Results and Discussions

The schematic diagram in Fig. 1A shows the bioprinting procedure. The vascular model was designed using the BIOCAD software. A 10-layer vascular construct having an internal diameter of 2.5 mm and a height of 3 mm was bioprinted using 2 printheads, one with Coll-HA hydrogel embedded EPC and second with Coll-HA hydrogel embedded SPC. After each layer, the polymerization module was inserted. The Coll-HA hydrogel polymerization was performed by exposure to UV for 5 seconds / layer. Working pressure has been established according to the physicochemical properties of the printed hydrogels. The optimal pressure was 1.1 - 1.2 bar (Fig. 1C). Printhead speed is a very important parameter for printing, and is dependent on the physicochemical properties of the hydrogels. At a too high speed it does not close the vascular structure, and at a low speed it creates a thick layer that leads to the formation of a vascular construct over the desired size. The printing speed was set at 1 mm / sec using a needle with 0.2 mm internal diameter. For optimum printing, the hydrogels were printed at 18°C, with the 3D bioprinter (3D Discovery, RegenHu, Switzerland) which have the possibility to adjust the printhead temperature. Using these parameters, were bioprinted vascular constructs with an internal diameter of 2.46 mm (± 0.41), wall thickness of 1.4 mm (± 0.10) and a height of 2.79 mm (± 0.05) (Figure 1B). These results show that the Coll-HA hydrogels can be used for vascular constructs and meet the desired requirements for reproduce with accuracy the model created in the BIOCAD software.

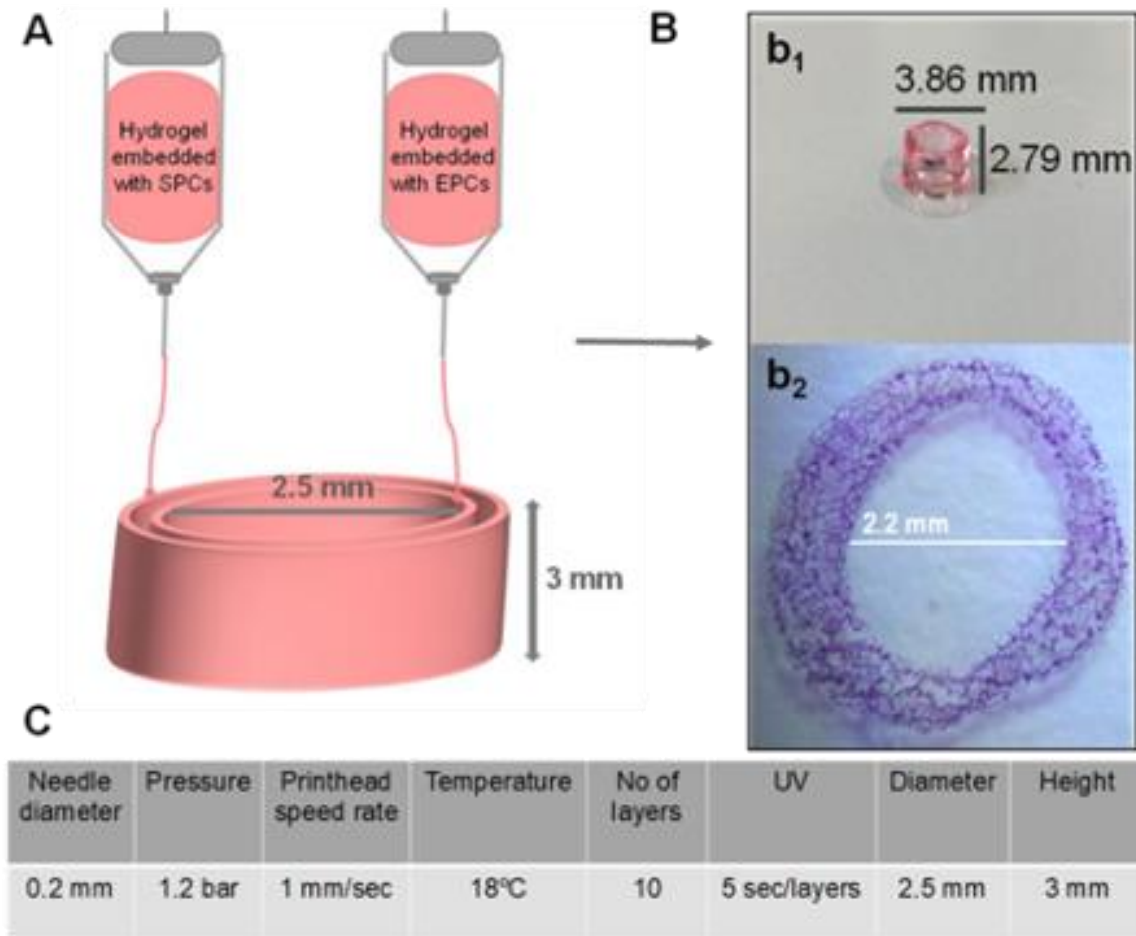


Fig. 1 Schematic diagram of bioprinting constructs (A) and optimal printing parameters of collagen-hyaluronic acid hydrogels based vascular construct (C). Macroscopic morphology (B, b₁) and H&E section of vascular constructs (B, b₂)

Other studies have shown that large wall thicknesses of vascular constructs may limit the transfer of oxygen and nutrients, while very small wall thicknesses would impair cells to align and spread reducing the mechanical strength [23, 24]. For these reasons, the nozzle made of a 0.2 mm internal needle was chosen for experiments, which were expected to meet both requirements for allowing sufficient nutrients diffusion and supporting cell growth. By optimizing the printer parameters, we continuously extruded smoothly hollow tubes with desired shapes and dimension.

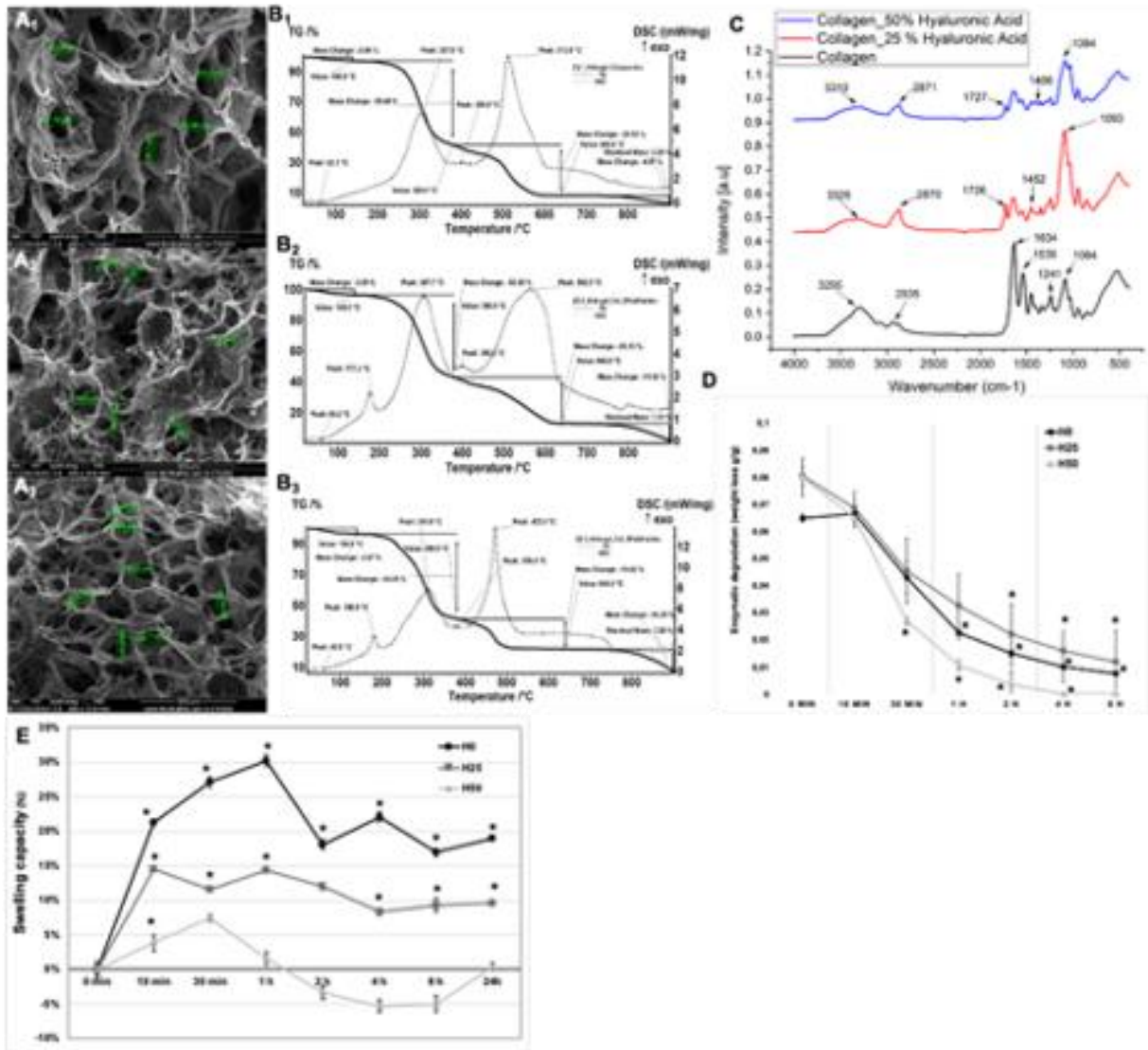


Fig. 2 Coll-HA hydrogels characterization by SEM (H0-A₁; H25-A₂; H50-A₃), TGA (H0-B₁; H25-B₂; H50-B₃), FTIR (C), enzymatic degradation (D), swelling capacity (E).

The morphology of Coll-HA hydrogels was assessed by SEM. The hydrogels present a characteristic porous morphology, the pore size was $107 \mu\text{m} \pm 23 \mu\text{m}$ for H0 hydrogel (Fig. 2 A₁), $51 \mu\text{m} \pm 20 \mu\text{m}$ for H25 hydrogel (Fig. 2 A₂), and $91 \mu\text{m} \pm 7 \mu\text{m}$ for H50 hydrogel (Fig. 2 A₃). The number and pore size are essential for cell growing, proliferation and adhesion, it has been considered that a pore size between 40-200 μm is appropriate to create an adequate microenvironment for cell development and tissue formation [25].

The hydrogel loses 2.66% of the mass in the RT-140°C interval, the process being accompanied by an endothermic effect with a minimum of 62.3°C. In the interval 140-380°C the sample suffers a mass loss of 55.46%, the process being accompanied by a strong, wide exothermic effect, with a maximum at 307.8°C. This is a process of oxidative degradation (parts of organic compounds are oxidized and at the same time chain breaks occur). In the range of 380-440°C there is a slower loss of mass, accompanied by a series of exothermic effects, superimposed, of lower intensity, indicating oxidation of some organic residues. Furthermore, the carbon mass remaining after oxidation undergoes a combustion process at CO₂ up to 640°C. This burning process is accompanied by an exothermic effect, very intense, slightly asymmetrical with a maximum of 513°C. The weight loss over the entire range is 33.53%. After 800°C the sample loses 4.87% of the initial mass, the residue representing 3.2% (Fig.2 B₁). The hydrogel with 25% hyaluronic acid is similar to the previous one, except for the exothermic effect at 177.3°C, which could be due to a reaction that takes place between hyaluronic acid and collagen (Fig.2 B₂). The hydrogel with 50% hyaluronic acid also retains a higher mass of residue between 650-850°C (Fig.2 B₃), suggesting the role of hyaluronic acid in stability of hydrogels.

In order to determine the presence of the functional groups characteristic of the compounds used in the material synthesis, the FT-IR analysis was performed on the samples of collagen, collagen and 25% hyaluronic acid and respectively collagen and 50% hyaluronic acid. The spectrum obtained in figure 2C shows the absorption bands in the range 4000-400 cm⁻¹.

The FTIR spectrum for the collagen hydrogel shows its specific absorption bands at 3295 cm⁻¹ representing amide A and at 2935 cm⁻¹ representing amide B. At the wave number 1634 cm⁻¹ is present amide I characterized by the presence of groups C = O. 1539 cm⁻¹ is the wave number assigned to amide II, where the vibration for the N-H and C-N groups is present, respectively. The case of the wave number 1241 cm⁻¹ shows the appearance of amide III correlated with the C-N and N-H vibrations. The absorption band at 1084 cm⁻¹ is characteristic of the tensile vibration of the C-O bond (Fig. 2C).

The presence of hyaluronic acid in the analyzed samples can be observed in comparison with the spectrum obtained for the collagen control sample.

The absorption band from approximately 3325 cm⁻¹ (for the sample with 25% hyaluronic acid) and 3310 cm⁻¹ (for the sample with 50% hyaluronic acid) is assigned to the OH and NH groups present in the structure of hyaluronic acid.

At the wave number of approximately 2870 cm^{-1} the vibration characteristic of the C-H group is observed. The value of the wave number of approximately 1400 cm^{-1} is attributed to the COO-characteristic extent of the acid group in hyaluronic acid. At about 1080 cm^{-1} the C-OH group is highlighted. The spectra recorded for the hyaluronic acid samples indicate at the wave number of approximately 1726 cm^{-1} the presence of the carboxyl groups C = O (Fig. 2C).

Enzymatic degradation of the constructs was revealed using type I collagenase and hyaluronidase. Bioprinted vascular constructs were immersed in culture medium (control constructs) and in collagenase type I and hyaluronidase medium ($10\text{ }\mu\text{g / ml}$) and weighed at different intervals of time (10 min, 30 min, 1 hour, 2 hours, 4 hours, and 8 hours). The results showed a 33,8% weight loss at 30 minutes, followed by 34,6% at 1 hour, 76,9% at 2 hours, 84,6% at 4 hours and 88,4% at 8 hours for collagen H0 construct (Fig. 2D). The H25 construct weight loss of 43,4 % of mass after 30 minutes, followed by 40,3% after 1 hour, 27,3% after 2 hours, 19% after 4 hours and 14% after 8 hours in the presence of collagenase type I and hyaluronidase. The most biodegradable construct was H50, after 4 hours entire construct was disintegrated in the medium (Fig. 2D).

The swelling capacity experiments showed that the H0 construct absorbs maximum of PBS at 1 hours after immersion, having a weight gain of 30,2% against the control construct. At 2-24 hours the values remain between 16-22%. In H25 construct swelling capacity is lower than in H0 construct, the maximum weight gain being 14,3% after 1 hour in the PBS (Fig. 2E). Furthermore, the H50 construct showed the lowest swelling capacity, with just 7,4% weight gain after 30 minutes in PBS (Fig. 2E). These results suggest that hyaluronic acid liberate water from the construct.

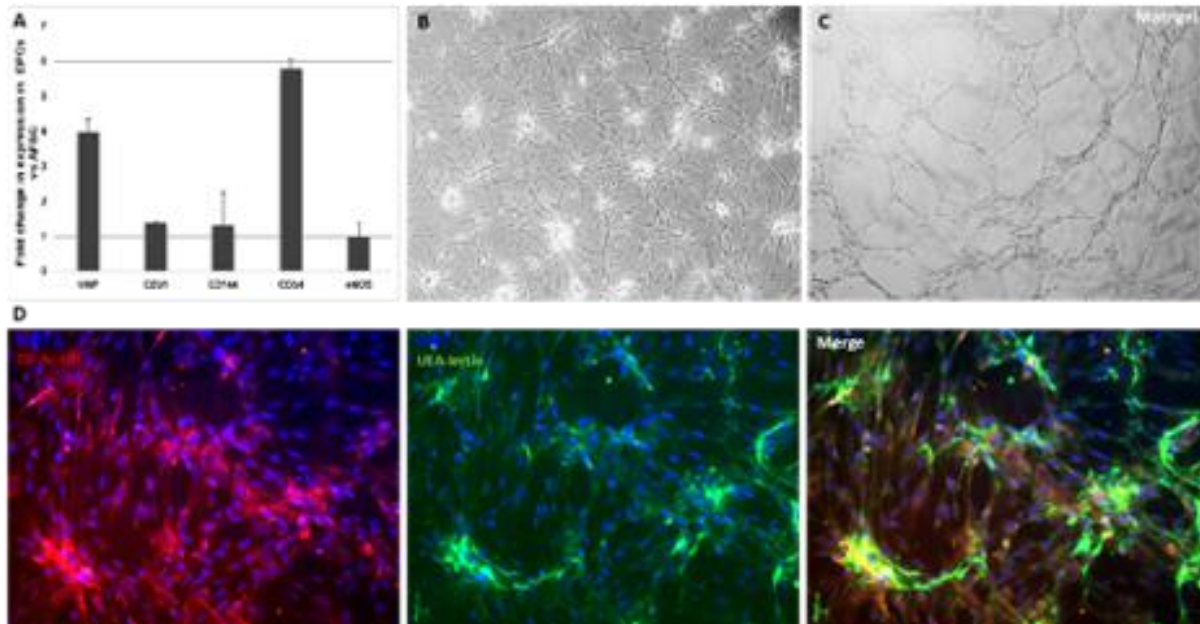


Figure 3. Characterization of differentiated EPC from amniotic fluid stem cells. A. qRT-PCR for detection of specific endothelial markers. B. Optical microscopy images of EPC cultures developed at 14 days in the presence of specific growth factors. C. Matrigel vascular tubes assay to evaluate the formation of blood vessel networks. D. Fluorescence images of EPC incorporating Dil-Ac-LDL and binding UEA-lectin.

Differentiation of EPC from AFSC was occurs after 10 days cultivation in endothelial specific medium supplemented with 40 ng/mL VEGF, 20 ng/ml IGF-1, 10 ng/ml EGF, and 10 ng/ml bFGF. After 10 days cells change the morphology from a fibroblast-like phenotype to an epithelia-like phenotype (Fig. 3B). The cells start to express endothelial specific markers such as vWF, CD31, CD144, CD54 and eNOS (Fig. 3A). The differentiate AFSC are capable to form vascular networks when are cultivate on Matrigel (Fig. 3C). Furthermore, these cells are capable to incorporating Dil-Ac-LDL and binding UEA-lectin (Fig. 3D), suggesting un endothelia cell phenotype.

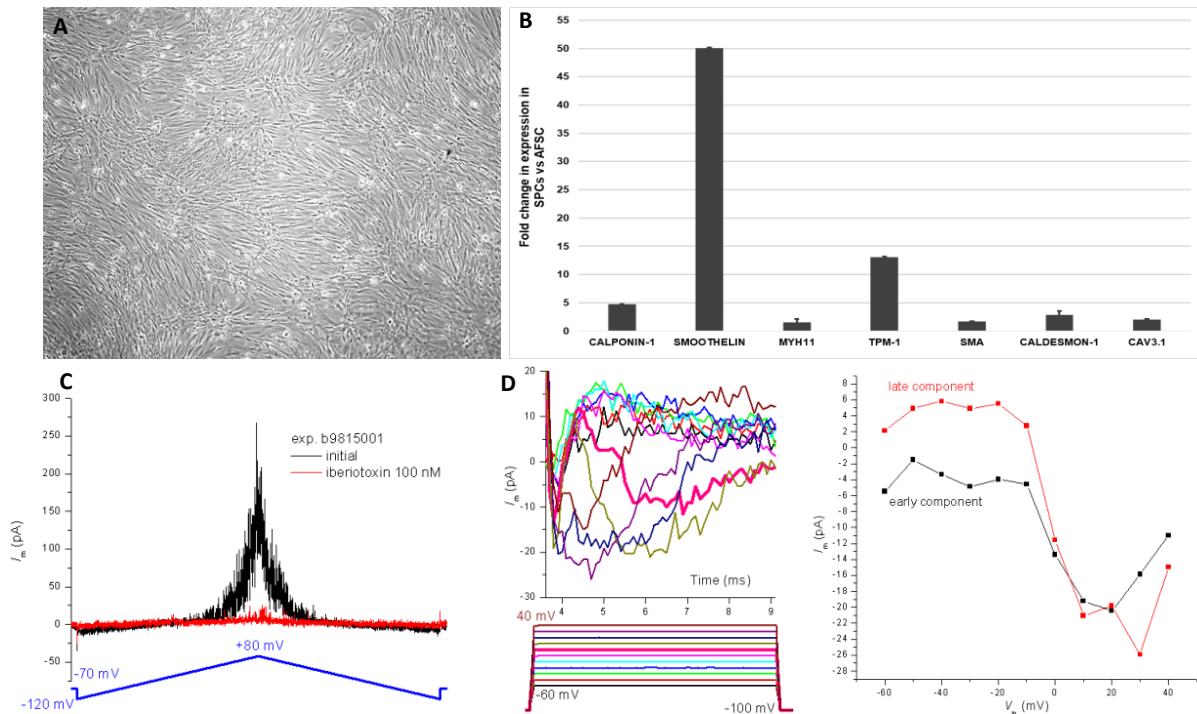


Figure 4. Characterization of differentiated SPC from amniotic fluid stem cells. A. Optical microscopy images of SPC cultures developed at 14 days in the presence of specific growth factors. B. qRT-PCR for detection of specific endothelial markers. C. Inhibitory effect of 100 nM iberiotoxin on BK current fluctuations at positive potentials, highlighted by a double-ramp voltage-clamp protocol. D. Inward current components suggestive of I_{CaT} and I_{CaL} .

Differentiation of SPC from AFSC was occurs after 10 days cultivation in smooth muscle specific medium supplemented with FGF (2 ng/ml), EGF (0.5 ng/ml), heparin (5 ng/ml), IGF (2 μ g/ml) and bovine serum albumin BSA (0.2 μ g/ml). After 10 days in culture cells presents a specific morphology, with a fusiform shape (Fig. 4B). The cells start to express smooth muscle markers such as calponin-1, smoothelin, myh11, tpm-1, SMA, caldesmon-1, cav3.1 (Fig. 4B). Furthermore, using a double-ramp voltage-clamp protocol we demonstrate the presence of BK current fluctuations at positive potentials (Fig. 4C) and inward current components suggestive of I_{CaT} and I_{CaL} calcium channels (Fig. 4D).

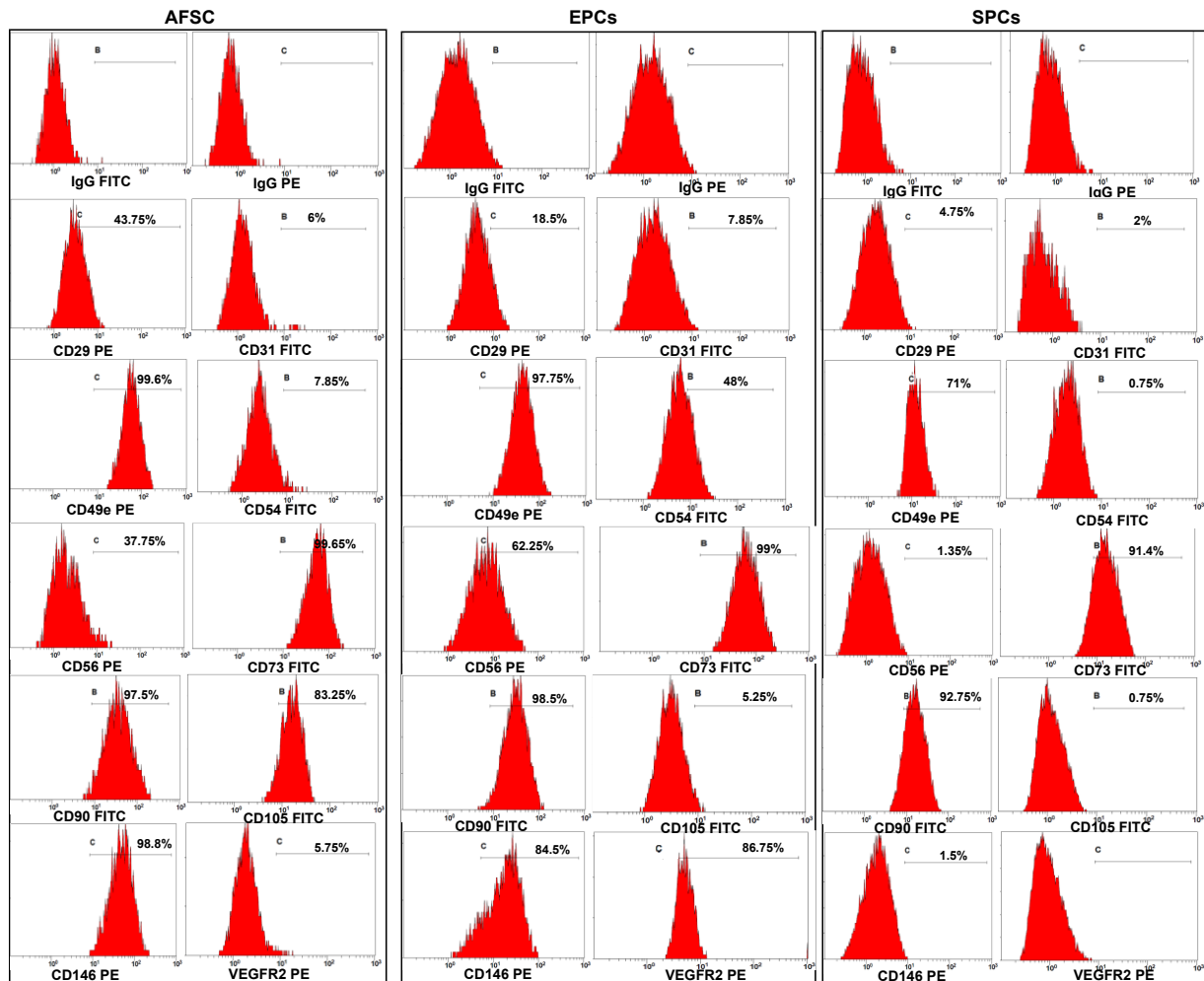


Figure 5. The immunophenotype of differentiated EPC and SPC from amniotic fluid stem cells after 10 day in the presence of specific growth factors

AFSC cultured in BIOAMF medium exhibits a mesenchymal phenotype characterized by surface markers CD29 (43,75%), CD49e (99.6%), CD54 (99,65%), CD56 (37,75%), CD73 (99.65%), CD90 (97,5%), CD 105 (83,25%) and CD146 (99,8%) (Fig. 5). CD29 is $\beta 1$ integrin, associates with integrin $\alpha 1$ and $\alpha 2$ forming collagen receptors. It is expressed on the surface of mesenchymal cells and generally on the surface of the adherent cells where it binds the actin cytoskeleton with the extracellular matrix and transmits two-way signals between the extracellular matrix and the cytoplasm. Homing cellular adhesion molecule (HCAM) is a surface glycoprotein involved in cell-cell interactions in cell adhesion and migration.

CD44 may also function as a receptor for hyaluronic acid and may interact with other ligands such as osteopontin, collagen and matrix metalloproteinases. CD49e is $\alpha 5$ integrin which in combination with $\beta 1$ integrin forms the fibronectin receptor. CD56 (NCAM) is part of the adhesion molecule family being neuronal cells. Data from the literature and previous results have shown that AFSC have an increased potential for differentiation in neural cells, so the medium in which they are cultivated and the duration of cell cultures is very important [13]. CD73 and CD90 are markers specific to mesenchymal adherent cells.

AFSC in the presence of EGM-2 medium supplemented with 40 ng / ml VEGF, 20 ng / ml IGF-1, 10 ng / ml EGF, 10 ng / ml β FGF showed the presence of endothelial cell-specific surface markers after 2 weeks. Flow cytometry assay revealed endothelial cell markers present on the surface of cells: CD31 (8%), CD54 (48%), CD146 (84,5%), VEGFR2 (86,75%) (Fig. 5). CD31 (platelet endothelial cell adhesion molecule) is a platelet and endothelial cell specific adhesion molecule involved in angiogenesis, vasculogenesis, integrin activation and leukocyte migration. Intercellular adhesion molecule 1 (ICAM-1) is an immunoglobulin family glycoprotein mediated on the surface of immune and endothelial cells, facilitating transmigration of leukocytes through vascular endothelium. CD105 (endoglin) is a protein involved in angiogenesis being found on the surface of vascular and endothelial progenitor cells.

AFSC growth in smooth muscle specific media, present only CD49e (71%), CD56 (91,4%) and CD73 (92,7%), suggesting a modification of protein expression towards a specific cell type (Fig. 5).

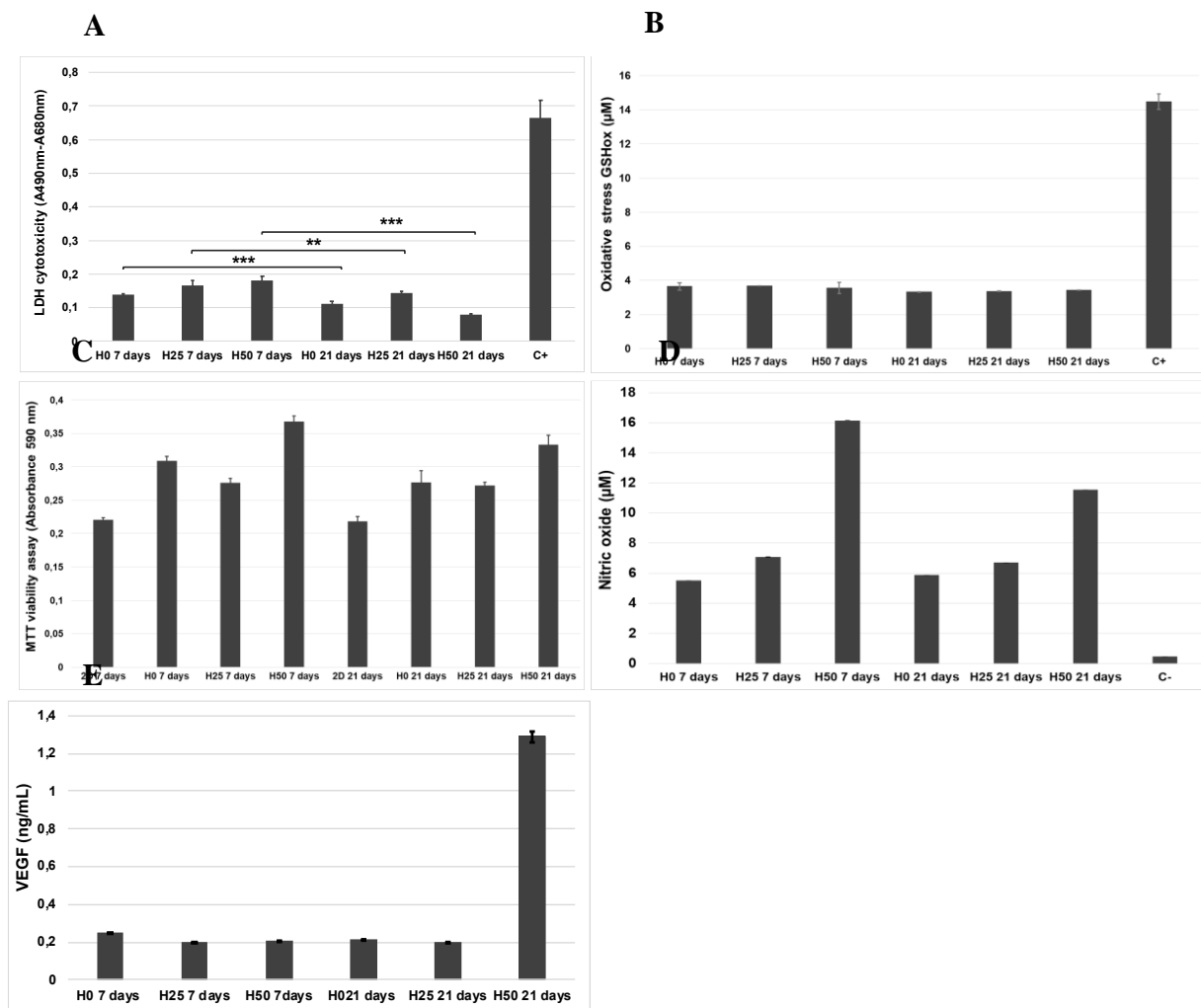


Figure 6. Characterization of blood vessel constructs populated with EPC and SMP. A. LDH viability assay, B. oxidative stress assays, C. MTT proliferation assay, D. Nitric oxide assay, E. ELISA assay for determination of VEGF

Characterization of blood vessel constructs populated with EPCs and SMPs was assessed using biochemical assays. EPC and SMP behavior at 7 and 21 days after bioprinting was evaluated using LDH, GSH, and MTT assays, as well as and SEM. Cellular viability after 7 days and 21 days was evaluated using an LDH assay. The results showed a low level of LDH compare to control suggesting that the cells remain viable in the constructs. At 7 days the highest level of LDH was observed for H50 construct, and after 25 days becoming the lowest (Fig. 6A). Cellular stress was evaluated using GSH assay. The level of GSH was between 3.33-3.69 μM , not statistical

significant compare with the positive control, suggesting that cells are not subjected to oxidative stress (Fig. 6B). The proliferation of the EPC and SPC was evaluated MTT assay. At 7 days post cultivation compare to the number of cells cultivated in plate (2D system), the cells in the H50 constructs presents a greater proliferation, followed by the cells in the H0 and H25 constructs. After 21 days the greatest proliferation was observed in H50 constructs, followed by H0 and H25 constructs (Fig. 6C). The level of nitric oxide (NO) was measured spectrophotometrically at 548 nm using the Griess Reagent Kit. The highest levels of NO were detected in H50 constructs, at 7 and 21 days, being 16,15 μM and 11,54 μM respectively (Fig. 6D). In H25 constructs the levels of NO were 7,8 μM and 6,7 μM at 7 days and 21 days of cultivation. The levels of NO do not change very much at 7 days and 21 day respectively for H0 constructs, being between 5,5-5,8 μM (Fig. 6D). The secretion of VEGF-A from the endothelial progenitor cells at 7 days and 21 days in culture was measured using VEGF-A ELISA kit. The highest level of VEGF-A was observed in H50 constructs, with a value of 1,29 ng/ml, followed by 0,25 ng/ml for H0 construct, and 0,25 ng/ml for H25 constructs (Fig. 6E). The results suggest that the cells are viable, with an active metabolism, and committed to EPC and SPC, being capable to secrete NO and VEGF.

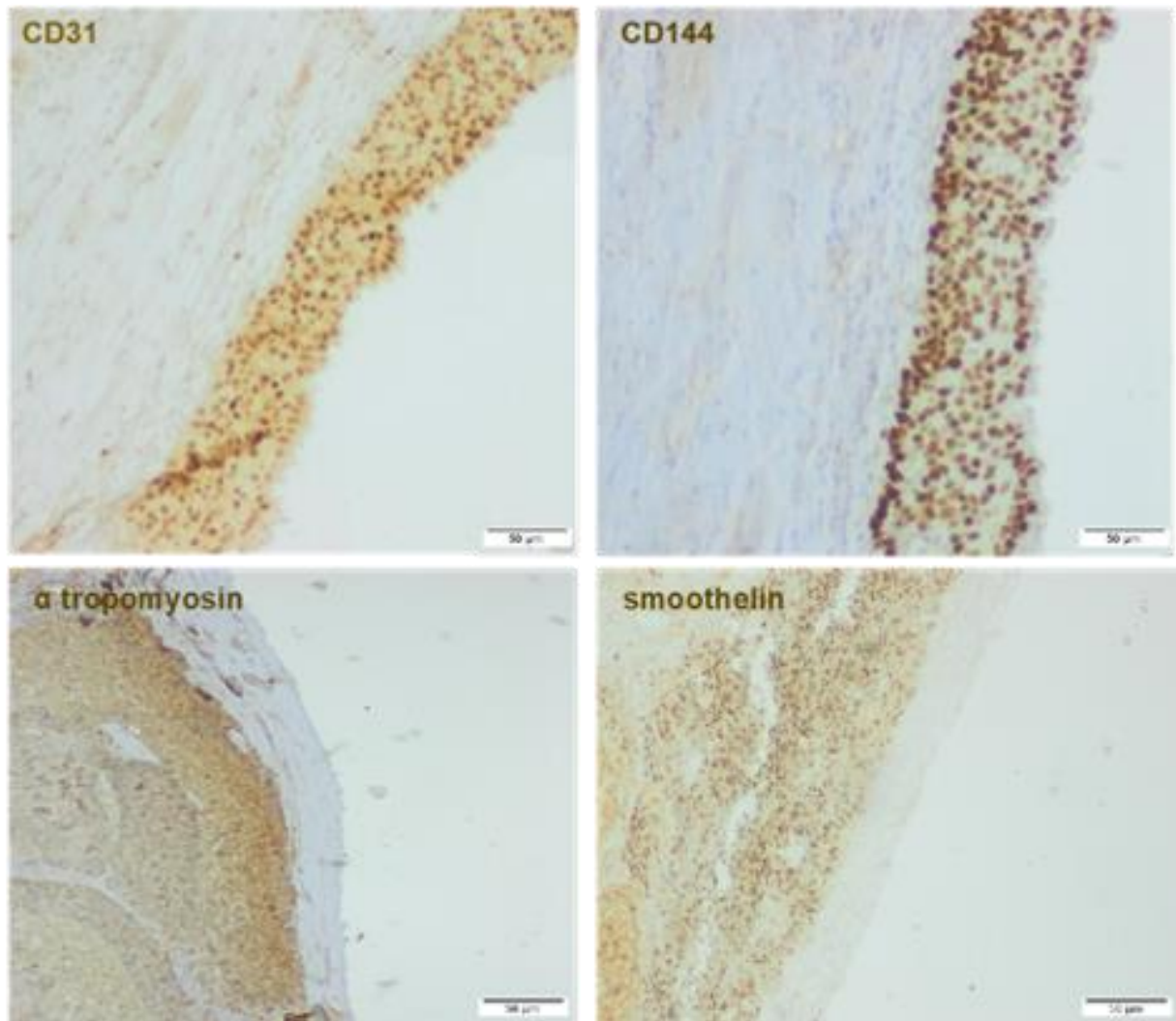


Figure 7. Immunohistochemistry of the constructs populated with EPC and SPC after 21 day in culture.

Immunohistochemistry was performed on 5 μ m-thick cryosections on constructs at 21 days post-bioprinting. The sections were then incubated overnight, at 4°C, with the following primary antibodies CD31, CD144, smoothelin, tropomyosin. The results showed that the cells expressed these endothelial and smooth muscle markers. Furthermore, immunohistochemistry images showed that the cells growth as they were bioprinted, observing the difference between external (muscle) layers, stained positive for tropomyosin and smoothelin and internal (endothelial) layers, stained positive for CD31 and CD144 (Fig. 7).

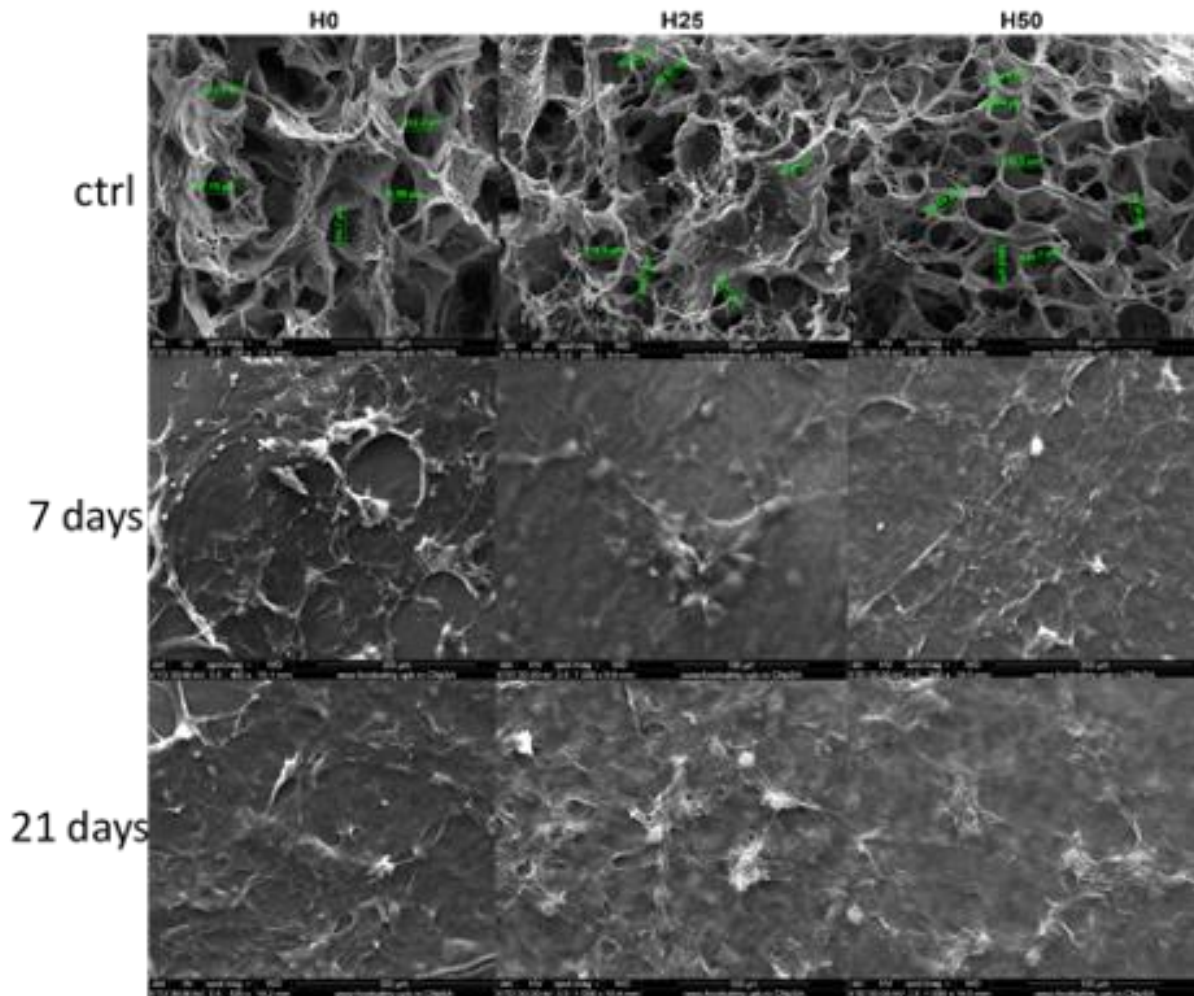


Fig. 8 Scanning electron microscopy images of H0, H25 and H50 hydrogels populated with EPC and SPC at 7 days and 21 days

The results showed that the cells adhere and distribute evenly in the collagen and hyaluronic acid hydrogels, which demonstrates the biocompatibility of these hydrogels. The H0 hydrogel has a porous structure, forms large pores with a diameter between 80-150 μM , H25 has smaller pores, between 40-120 μM and H50 between 80-150 μM . In the presence of the H0 hydrogel, the cells have a fusiform morphology and emit filopods that allow the cells to interact with each other and with the collagen fibres. The H25 and H50 hydrogels allow a good growth of cells, forming a rich extracellular matrix which allows a good adhesion and the possibility of organizing in a tissue (Fig. 8).

In conclusion, these results showed that the collagen/hyaluronic acid hydrogels allows the creation of the vascular constructs; the parameters of the 3D bioprinter have been optimized so that a vascular structure similar to the model developed in the BIOCAD program can be created. Amniotic fluid isolated cells are mesenchymal stem cells with potential for differentiation to endothelial and smooth muscle cells. The collagen-hyaluronic acid hydrogels are biocompatible with the EPC and SPC. The obtained results showed that in the vascular structures created the cells are viable, proliferate and secrete factors necessary for the formation of blood vessels. The cells in the vascular structures express markers specific to the endothelial and muscular cells, suggesting the possibility of vascular graft formation.

References

1. Thomas J.D. Could 3D bioprinted tissues offer future hope for microtia treatment. *International Journal of Surgery*, 32, 43-44, 2016
2. Iordache, F., 2019. *Hydrogels and Polymer-based Scaffolds, Chapter 2: Bioprinted scaffolds*. Elsevier Academic Press, USA.
3. Chua C.K., Yeong W.Y. *Bioprinting: Principles and Applications*. Singapore: World Scientific Publishing Co., 2015.
4. Datta P, Ayan B, Ozbolat IT. Bioprinting for vascular and vascularized tissue biofabrication. *Acta Biomaterialia* 51, 1–20, 2017.
5. Abdulrazzak H, De Coppi P, Guillot PV. Therapeutic potential of amniotic fluid stem cells. *Curr Stem Cell Res Ther.* 8(2):117-24, 2013.
6. Pozzobon M, Piccoli M, Schiavo AA, Atala A, De Coppi P. Isolation of c-Kit+ human amniotic fluid stem cells from second trimester. *Methods Mol Biol.* 1035:191-8, 2013.
7. Pipino C, Pierdomenico L, Di Tomo P, Di Giuseppe F, Cianci E, D'Alimonte I, Morabito C, Centurione L, Antonucci I, Marigliò MA, Di Pietro R, Ciccarelli R, Marchisio M, Romano M, Angelucci S, Pandolfi A. Molecular and phenotypic characterization of human amniotic fluid-derived cells: a morphological and proteomic approach. *Stem Cells Dev.* 24(12):1415-28, 2015.
8. Cananzi M, De Coppi P. CD117+ amniotic fluid stem cells: State of the art and future perspectives. *Organogenesis* 8:3, 77-88, 2012.
9. Benavides OM, Quinn JP, Pok S, Petsche Connell J, Ruano R, Jacot JG. Capillary-Like Network Formation by Human Amniotic Fluid-Derived Stem Cells Within Fibrin/Poly(Ethylene Glycol) Hydrogels. *Tissue Eng Part A.* 21(7-8):1185-94, 2014.
10. Connell JP, Ruano R, Jacot JG. Amniotic fluid-derived stem cells demonstrate limited cardiac differentiation following small molecule-based modulation of Wnt signaling pathway. *Biomed Mater.* 10(3):034103, 2015.
11. Resca E, Zavatti M, Maraldi T, Bertoni L, Beretti F, Guida M, La Sala GB, Guillot PV, David AL, Sebire NJ, De Pol A, De Coppi P. Enrichment in c-Kit improved differentiation potential of amniotic membrane progenitor/stem cells. *Placenta.* 36(1):18-26, 2015.
12. Spinelli V, Guillot V.P., De Coppi P. Induced pluripotent stem (iPS) cells from human fetal stem cells (hFSCs). *Organogenesis*, 9(2):101–110, 2013.

13. Mirabella T, Hartinger J, Lorandi C, Gentili C, van Griensven M, Cancedda R. Proangiogenic soluble factors from amniotic fluid stem cells mediate the recruitment of endothelial progenitors in a model of ischemic fasciocutaneous flap. *Stem Cells Dev.*, 21(12):2179-2188, 2012.
14. D. Mozaffarian, E. J. Benjamin, A. S. Go, D. K. Arnett, M. J. Blaha, M. Cushman, S. R. Das, S. de Ferranti, J. P. Despres, and H. J. Fullerton, *Circulation* 133(4), e38 (2016).
15. J. D. Lee, M. Srivastava, and J. Bonatti, *Circ. J.* 76(9), 2058 (2012)
16. B. C. Isenberg, C. Williams, and R. T. Tranquillo, *Circ. Res.* 98(1), 25 (2006).
17. L. Dall’Olmo, I. Zanusso, R. Di Liddo, T. Chioato, T. Bertalot, E. Guidi, and M. T. Conconi, *Biomed. Res. Int.* 2014, 685426
18. A. Hasan, A. Memic, N. Annabi, M. Hossain, A. Paul, M. R. Dokmeci, F. Dehghani, and A. Khademhosseini, *Acta. Biomater.* 10(1), 11 (2014).
19. Z. H. Syedain, M. L. Graham, T. B. Dunn, T. O’Brien, S. L. Johnson, R. J. Schumacher, and R. T. Tranquillo, *Sci. Trans. Med.* 9(414), ean4209 (2017).
20. D. G. Seifu, A. Purnama, K. Mequanint, and D. Mantovani, *Nat. Rev. Cardiol.* 10(7), 41, 2013.
21. J. Jang, J. Y. Park, G. Gao, and D.-W. Cho, *Biomaterials*, 156, 88 (2018).
22. Bolotina VM, Najibi S, Palacino JJ, Pagano PJ, Cohen RA. Nitric oxide directly activates calcium-dependent potassium channels in vascular smooth muscle. *Nature.* 1994; 368:850–853.
23. Y. Zhang, Y. Yu, H. Chen, I.T. Ozbolat, Characterization of printable cellular micro-fluidic channels for tissue engineering, *Biofabrication* 5 (2013) 025004.
24. Jia W, Gungor-Ozkerim PS, Zhang YS, Yue K, Zhu K, Liu W, Pi Q, Byambaa B, Dokmeci MR, Shin SR, Khademhosseini A. Direct 3D bioprinting of perfusable vascular constructs using a blend bioink. *Biomaterials.* 2016 Nov;106:58-68.
25. Katia Jarquín-Yáñez, Jesús Arenas-Alatorre, Gabriela Piñón-Zárte, Rosa María Arellano-Olivares¹, Miguel Herrera-Enríquez, Beatriz Hernández-Téllez, Andrés E Castell-Rodríguez. Structural Effect of Different EDC Crosslinker Concentration in Gelatin- Hyaluronic Acid Scaffolds. *J Bioengineer & Biomedical Sci.*6:2, 1-6, 2016.

30.10.2020

Project director,

Dr. Florin Iordache

